LA-UR-12-25524
Approved for public release; distribution is unlimited.

Title: SESAME 96171, a three-phase equation of state for CeO2

Author(s): Chisolm, Eric D.

Intended for: Report

Issued: 2014-07-08 (rev.1)

SESAME 96171, a three-phase equation of state for CeO_2

Eric D. Chisolm
Theoretical Division, Los Alamos National Laboratory, Los Alamos, NM 87545

This report describes an earlier version of an equation of state (EOS) for cerium (IV) oxide, CeO_2. This work has been superseded by a newer version that is described in LA-UR-14-24689. Everything from this report needed to understand the new version is included in the new report.

I. INTRODUCTION

Previously I constructed an equation of state (EOS) for cerium (IV) oxide (CeO_2) that included the ambient cubic fluorite phase and the liquid [1]. However, diamond anvil cell data from Duclos et al. show a transition to a high-pressure solid phase at about 31 GPa that exhibits a $7-8\%$ volume collapse [2]. To include this phase, I have made an explicit multiphase EOS for this material: such an EOS is built by creating separate EOS for the ambient solid, high-pressure solid, and liquid phases, determining the phase boundaries by matching Gibbs free energies, and then combining all three EOS into a single SESAME table. (The single table would be used in hydrodynamic simulations that assume the material is in thermodynamic equilibrium at all times; alternately, the EOS of the three phases separately can be used with a kinetic model to allow non-equilibrium transitions between phases.)

II. MODELS AND PARAMETERS

The basic parameters for the EOS, as before, are the atomic number Z, atomic weight A, and reference density $\rho_{\rm ref}$ (the density at ambient conditions). Also as before, the atomic number and weight represent an "average atom" of CeO_2, and their values are listed in Table I. For each phase, I construct a Helmholtz free energy per

$$\begin{aligned} Z &= 24.6667 \\ A &= 57.3716 \\ \rho_{\rm ref} &= 7.215 \text{ g/cm}^3 \end{aligned}$$

TABLE I: The basic EOS parameters.

unit mass, from which I determine pressure and energy as explained in Ref. [1]. The models used in each phase's EOS are similar to those used in the previous EOS; here I will only report the parameters used and indicate any changes required for the multiphase construction. The strategy I follow is the one described in Ref. [3]; the liquid is modeled on one of the solid phases to control the location of the melt curve. In this case, I choose to model the liquid on the low-pressure solid phase for reasons described in Section II C below.

A. The low-pressure solid

The cold curve interpolates between a Lennard-Jones form at low densities, $T = 0$ Thomas-Fermi-Dirac (TFD) at high densities, and the Rose-Vinet form inbetween. The parameter values I used are given in Table II, and they have the same meaning as the parameters in Ref. [1]. Almost all of them have been modified from the previous EOS, to slightly improve the agreement with experimental data.

$$\begin{aligned} a_4 &= 1.0 \\ E_{\rm coh} &= 120 \text{ kcal/mol} \\ \rho_{\rm lo} &= 6.85425 \text{ g/cm}^3 \\ \phi_* &= 0 \text{ MJ/kg} \\ \rho_* &= 7.3091 \text{ g/cm}^3 \\ B_* &= 246.2 \text{ GPa} \\ B'_* &= 4 \\ \rho_{\rm hi} &= 18.0375 \text{ g/cm}^3 \end{aligned}$$

TABLE II: The parameter values for the low-pressure solid cold curve.

The nuclear contribution for a solid phase of a multiphase EOS presents a challenge. Our present procedure is to construct a solid EOS that covers the entire SESAME range, for most of which it is not the stable phase. Therefore the EOS should have the proper solid behavior in its intended region of stability, but at high temperatures it should yield its place to the liquid. Since the specific heat of a liquid is roughly $3/2\,R$ per mole while a solid is roughly $3R$ per mole, if the solid EOS keeps its solid-like specific heat at high temperatures its Gibbs free energy will necessarily be lower, so it will reassert itself as the stable phase. Therefore even the solid EOS must exhibit liquid-like behavior at high temperatures. To achieve this, I use a model for a liquid's nuclear contribution [3], with one modification. The model allows me to set the entropy of melting of the liquid, and for this phase I set it to zero. (See Table III.) This gives me the required behavior at low temperatures, and the Gibbs free energy gracefully increases at higher temperatures to prevent re-emergence of the phase. Although the exact equations are different, the model follows a very similar philosophy to the nuclear model used before. One practical difference is that, although the melt curve is still

a Lindemann form, the model does not fix its normalization. Therefore the choice of melt temperature at one density does not normalize $\theta(\rho)$, so it must be done separately. The new parameter $\theta(\rho_g)$ in Table III does this. The model for the Grüneisen parameter used in this EOS is the same model that was used in the previous EOS. As with the cold curve, many of the parameters have been tweaked to improve the fit with experimental data.

$$\begin{aligned}
\rho_{\rm melt} &= 6.573 \text{ g/cm}^3 \\
T_m(\rho_{\rm melt}) &= 4975 \text{ K} \\
\Delta S &= 0\,k_B/\text{atom} \\
\rho_g &= 7.215 \text{ g/cm}^3 \\
\theta(\rho_g) &= 625 \text{ K} \\
\Gamma(\rho_g) &= 2.75 \\
\Gamma_0 &= 1.0 \\
\Gamma_\infty &= 0.6667 \\
\frac{d\Gamma}{d\ln\rho}(\rho_g) &= -2.0
\end{aligned}$$

TABLE III: The parameter values for the low-pressure solid nuclear model.

Because this phase is an insulator, I omit the thermal electronic term in this EOS, as I said I planned to in Ref. [1]. That completes the Helmholtz free energy for this phase, and the other thermodynamic functions follow in the standard way.

B. The high-pressure solid

The only data I have for the high-pressure solid is the room temperature isotherm from diamond anvil cell; this tells me the location of the phase boundary and gives me some information about the density and bulk modulus of the new phase. I'll compare with that data in Section III, but for now I just give the EOS parameters.

The cold curve is the same combination of models as it was for the first solid phase, and the parameters are given in Table IV. The new values of ρ_* and B_* were suggested by Duclos et al. [2], and the parameter ϕ_* was used to control the location of the phase boundary.

The nuclear model is the same one used for the low-pressure solid, with the same idea: we want proper solid-like behavior at low temperatures, while the liquid is stable at higher temperatures. The model parameters are given in Table V.

Since this phase represents the solid at arbitrarily high pressures, it is not physically reasonable to make it an insulator too (it is expected that all solids will become metals in the high-pressure limit). Therefore I use the same electronic contribution for this phase that I used in the previous EOS: an additive-volume mixture of TFD calculations for Ce and O separately in a 1 : 2 ratio by particle number [1]. This completes the EOS for the second solid phase.

$$\begin{aligned}
a_4 &= 0.9 \\
E_{\rm coh} &= 119 \text{ kcal/mol} \\
\rho_{\rm lo} &= 6.85425 \text{ g/cm}^3 \\
\phi_* &= 0.38 \text{ MJ/kg} \\
\rho_* &= 8.096 \text{ g/cm}^3 \\
B_* &= 325 \text{ GPa} \\
B'_* &= 3.9 \\
\rho_{\rm hi} &= 18.0375 \text{ g/cm}^3
\end{aligned}$$

TABLE IV: The parameter values for the high-pressure solid cold curve.

$$\begin{aligned}
\rho_{\rm melt} &= 6.573 \text{ g/cm}^3 \\
T_m(\rho_{\rm melt}) &= 2750 \text{ K} \\
\Delta S &= 0\,k_B/\text{atom} \\
\rho_g &= 7.95 \text{ g/cm}^3 \\
\theta(\rho_g) &= 625 \text{ K} \\
\Gamma(\rho_g) &= 2.75 \\
\Gamma_0 &= 1.0 \\
\Gamma_\infty &= 0.6667 \\
\frac{d\Gamma}{d\ln\rho}(\rho_g) &= -2.0
\end{aligned}$$

TABLE V: The parameter values for the high-pressure solid nuclear model.

C. The liquid

The liquid is modeled on the low-pressure solid phase in the sense described in Ref. [3]. Therefore its cold curve is constructed in two steps. I start with the low-pressure solid cold curve, constructed using the models and parameters from Section II A and Table II, and I add to it a correction of the form

$$\Delta\phi(\rho) = \frac{RT_m(\rho)}{A}\Delta S \tag{1}$$

where R is the ideal gas constant, A is the atomic weight, $T_m(\rho)$ is an approximation to the intended melt curve and ΔS is the entropy of melt at constant volume. (ΔS will appear again as a parameter in the nuclear model; see below.) This shifts the Gibbs free energy of the liquid up at low temperatures, ensuring the stability of the solid phases there.

The nuclear model is the same model as used for the solid phases, with the same parameters as the low-pressure solid from Table III, with one exception: I now use $\Delta S = 0.8\,k_B/\text{atom}$, which is a standard value derived

from experimental data from a wide range of elements. Since the low-pressure solid and the liquid share nuclear parameters, data from both phases are used to determine them. All of the parameters except ΔS and $T_m(\rho_{\rm melt})$ are determined from low-pressure solid data, but $T_m(\rho_{\rm melt})$ was chosen to get the correct melt temperature at 1 atm.

Finally, since the liquid extends over the entire density range, it is not physically reasonable to make it an insulator either; therefore it includes the same electronic contribution as the high-pressure (but not the low-pressure) solid. This is the largest difference between the EOS of the two phases, and it is the only significant departure from the plan to model the liquid on the low-pressure solid.

I chose not to model the liquid on the high-pressure solid because the only experimental data I have for the liquid is for melt, and CeO_2 melts out of the low-pressure phase. I found that if I modeled the liquid on the high-pressure solid, the phase boundary between the liquid and the low-pressure solid was sufficiently ill-behaved that I couldn't get the correct melt temperature at 1 atm. The boundaries between the liquid and both solid phases ended up behaving reasonably, as I'll show below.

D. The multiphase EOS

The procedure for constructing a multiphase EOS from the EOS of the individual phases is described in Ref. [4]. At each point on the SESAME table grid we determine mass fractions $\lambda_i(\rho,T)$ and densities ρ_i for each phase that satisfy the conditions of minimizing the Gibbs free energy of the material while keeping the phases in pressure equilibrium. The total free energy is given by

$$F(\rho,T) = \sum_i \lambda_i(\rho,T) F_i(\rho_i,T), \tag{2}$$

with a similar equation for the internal energy; the pressure is simply the equilibrium pressure of the phases.

Since the functional forms of the phases are parameterized by data in their ranges of stability, sometimes the models produce Gibbs free energies that behave inappropriately, allowing phases to become stable again outside their regions of real stability. We partially address this issue in the temperature regime via the nuclear model I used for all phases, but the problem can occur for other reasons also. Because of this, I chose to exclude the low-pressure solid from the multiphase construction at densities below 6.0 g/cm^3 and the high-pressure solid at densities below 6.9 g/cm^3. Finally, I standardized the EOS by subtracting its energy at ambient conditions (1 atm and room temperature).

III. COMPARISON WITH DATA

The experimental data for CeO_2 used to construct and test this EOS are the same data that were used for the previous EOS. I used the data in Tables VI and VII together with three curves:

1. α_P versus T at 1 atm from Touloukian et al. [5] and Taylor [6]
2. C_P versus T at 1 atm from Westrum and Beale [7], King and Christensen [8], and Ricken et al. [9]
3. the DAC data from Duclos et al. [2]

The data in the tables and the location of the solid-solid phase transition were used to set the EOS parameters, and the curves were used as tests.

Quantity	Value	Reference
$\rho_{\rm ref}$	7.215 g/cm^3	[2]
α_P	2.92×10^{-5} K^{-1}	[5, 6]
C_P	3.58 MJ/kg/K	[7]
B_T	236 ± 4 GPa	[10]
B_T'	4.4	[10]

TABLE VI: Experimental data at ambient conditions ($P = 1$ atm, $T = 298$ K).

Quantity	Value	Reference
T_m	2750 K	[11]
T_b	3800 K	[12]

TABLE VII: Melting and boiling at $P = 1$ atm.

Figure 1 shows part of the phase diagram, including the 1 atm isobar. Melt occurs where the isobar crosses from the low-pressure solid to the liquid phase, at approximately 2750 K. It is not shown in the figure, but the isobar crosses the vapor dome at approximately 3800 K as required. The figure also shows the nonuniform gridding used in the EOS to allow more accurate interpolation in certain regions.

The vapor dome is a challenge for multiphase EOS. In general, if the phase boundaries extend into the expanded region, the resulting EOS does not have well-behaved van der Waals loops, and a Maxwell construction cannot be performed. In this case, I have restricted the solid phases to extend only slightly into expansion, so the EOS is mostly liquid. This is not enough to allow for a Maxwell construction, but it does mean that the vapor dome of the pure liquid EOS matches the vapor dome the multiphase EOS would have except for the highest densities on the liquid side. Therefore I have added the vapor dome table from the liquid EOS to the multiphase EOS, understanding that it is exactly correct at most points and close to correct at the remaining points.

Figure 2 shows the thermal expansion comparison. The two data sets have noticeably different trends at both low and high temperatures, and as before I attempted to capture both. All of this data is for the low-pressure solid, so the difficulties I outlined in Ref. [1] persist, despite

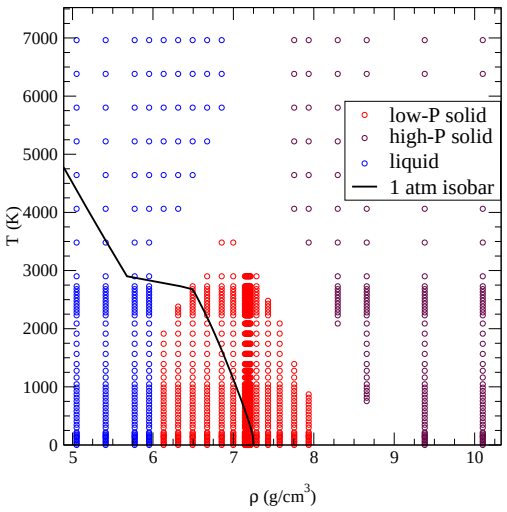

FIG. 1: The low-pressure phase diagram for SESAME 96171. The 1 atm isobar is also shown. The material melts at 1 atm at approximately 2750 K.

some improvements. In Figure 3, the low-temperature specific heat is very well reproduced, and omitting the low-pressure solid's electronic term has slightly lowered the high-temperature specific heat, bringing it closer to the data.

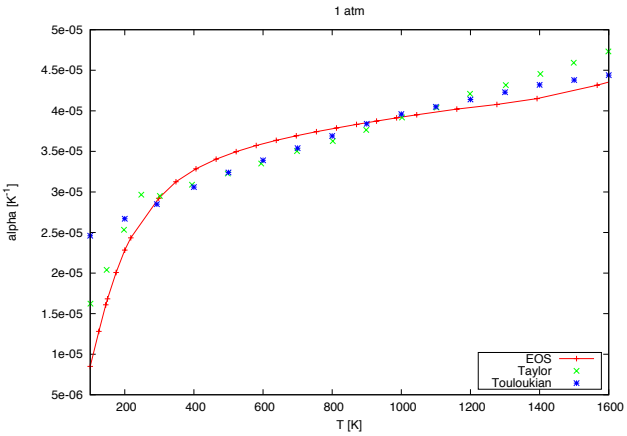

FIG. 2: The volume coefficient of thermal expansion α_P versus T at $P = 1$ atm. The prediction of SESAME 96171 is shown alongside data from Touloukian et al. [5] and Taylor [6].

The compression behavior of this EOS is much better than its predecessor, as shown by Figure 4. I chose to place the phase transition at 31 GPa, as suggested by

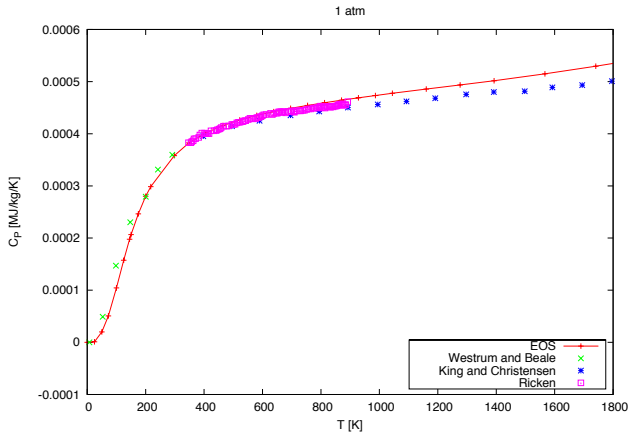

FIG. 3: Constant-pressure specific heat C_P versus T at $P = 1$ atm. The prediction of SESAME 96171 is shown alongside data from Westrum and Beale [7], King and Christensen [8], and Ricken et al. [9].

Duclos et al. [2], as they believe that some of their data exhibit a persistence of the low-pressure solid beyond its equilibrium stability range.

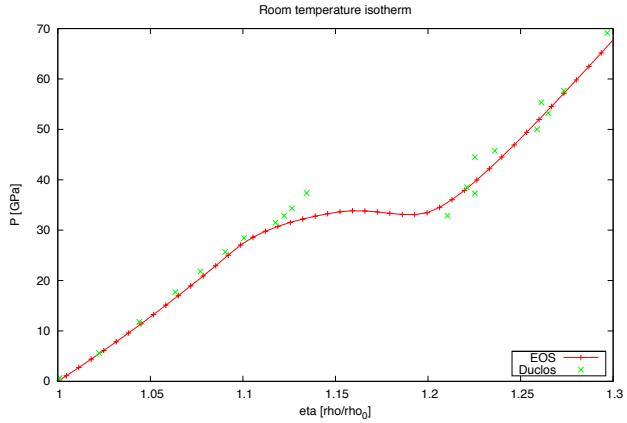

FIG. 4: Pressure at $T = 298$ K as a function of relative density. The prediction of SESAME 96171 is shown alongside data from Duclos et al. [2]. The EOS agrees with the data through both solid phases.

I am not yet able to compare meaningfully with porous Hugoniot data, as the problems outlined in the previous report have not yet been solved.

IV. CONCLUSIONS

I have constructed SESAME 96171, an EOS for cerium (IV) oxide that includes two solid phases and the liquid. Unlike its immediate predecessor, this EOS is valid over a larger range in pressure due to including the extra phase. I have described the process of constructing and testing the EOS, emphasizing its continuity with the previous EOS and the modifications needed for the new framework. The comparison with data is good, but is still limited by the same issues with nuclear models that were present in the previous work.

The remaining significant issue is the comparison of the crystal-density EOS with experimental porous Hugoniot data, which may require using more sophisticated models to represent porosity, as discussed in the previous report.

V. ACKNOWLEDGMENTS

This work was supported by the U. S. Department of Energy through contract DE-AC52-06NA25396.

[1] E. D. Chisolm, Los Alamos National Laboratory report LA-UR 12-21066, (2012).
[2] S. J. Duclos, Y. K. Vohra, A. R. Ruoff, A. Jayaraman, and G. P. Espinosa, Phys. Rev. B **38**, 7755 (1988).
[3] E. D. Chisolm, Los Alamos National Laboratory report LA-UR 10-08329, (2010).
[4] E. D. Chisolm, C. W. Greeff, and D. C. George, Los Alamos National Laboratory report LA-UR 05-9413, (2005).
[5] Y. S. Touloukian, R. K. Kibby, R. E. Taylor, and T. Y. R. Lee, *Thermophysical properties of matter, vol. 13. Thermal expansion of nonmetallic solids* (NY: Plenum, 1970).
[6] D. Taylor, Br. Ceram. Trans. J. **83**, 32 (1984).
[7] E. F. Westrum, Jr and A. F. Beale, Jr, J. Phys. Chem. **65**, 353 (1961).
[8] E. G. King and A. U. Christensen, U.S. Bur Mines Rep. Invest. **RI-5789**, 1 (1961).
[9] M. Ricken, J. Nölting, and I. Reiss, J. Solid State Chem. **54**, 89 (1984).
[10] L. Gerward and J. S. Olsen, Powder Diffr. **8**, 127 (1993).
[11] The Handbook of Chemistry and Physics Online, `http://www.hbcpnetbase.com/`.
[12] `http://en.wikipedia.org/wiki/Cerium(IV)_oxide`, accessed in 2012.